Bactericidal and membrane disruption activities of the eosinophil cationic protein are largely retained in an N-terminal fragment

Marc TORRENT*, Beatriz G. DE LA TORRE†, Victòria M. NOGUÉS*, David ANDREU† and Ester BOIX*[1]

*Department Bioquímica i Biologia Molecular, Facultat de Biociències, Universitat Autònoma de Barcelona, Cerdanyola del Vallès, Spain, and †Department Ciències Experimentals i de la Salut, Universitat Pompeu Fabra-Parc de Recerca Biomèdica de Barcelona, Barcelona, Spain

ECP (eosinophil cationic protein) is an eosinophil secretion protein with antipathogen activities involved in the host immune defence system. The bactericidal capacity of ECP relies on its action on both the plasma membrane and the bacterial wall. In a search for the structural determinants of ECP antimicrobial activity, we have identified an N-terminal domain (residues 1–45) that retains most of ECP's membrane-destabilizing and antimicrobial activities. Two sections of this domain, ECP-(1–19) and ECP-(24–45), have also been evaluated. All three peptides bind and partially insert into lipid bilayers, inducing aggregation of lipid vesicles and leakage of their aqueous content. In such an environment, the peptides undergo conformational change, significantly increasing their α-helix content. The bactericidal activity of the three peptides against *Escherichia coli* and *Staphylococcus aureus* has been assessed at both the cytoplasmic membrane and the bacterial envelope levels. ECP-(1–45) and ECP-(24–45) partially retain the native proteins ability to bind LPS (lipopolysaccharides), and electron microscopy reveals cell damage by both peptides. Interestingly, in the *E. coli* cells agglutination activity of ECP is only retained by the longest segment ECP-(1–45). Comparative results suggest a task distribution, whereby residues 1–19 would contribute to membrane association and destabilization, while the 24–45 region would be essential for bactericidal action. Results also indicate that ECP cytotoxicity is not uniquely dependant on its membrane disruption capacity, and that specific interactions at the bacteria wall are also involved.

Key words: antimicrobial peptide, electron microscopy, host defence, lipopolysaccharide, liposome.

INTRODUCTION

Host defence proteins and peptides of the innate immune system are potential candidates for chemotherapeutic development. Among those, AMPs (antimicrobial peptides) are characterized by a variety of primary and secondary structures [1] and by a broad spectrum of activity. Their fast non-specific mechanism of action [2], mostly at the plasma membrane and cell surface level, tends to mean the development of resistant strains is rather unlikely [3]. On the basis of these features, several native AMPs, or their synthetic analogues, have been proposed as alternatives to conventional antibiotics and some of them are currently in clinical trials, mostly for topical applications [4].

Some AMPs are derived from host defence proteins by limited proteolysis that releases *in vivo* active fragments, often corresponding to the N- or C-terminus [5]. Proteolytic processing is very frequent in immunological cascade events, where local cleavage can release the active peptides in the area of infection or inflammation. There are also multiple examples of synthetic peptides corresponding to a protein N- or C-terminus that display antimicrobial activity [6]. Thus lactoferricin, a naturally occurring bactericidal peptide derived from the N-terminus of lactoferrin, is very effective against some antibiotic-resistant strains [7]. Likewise, BPI (bactericidal permeability-increasing protein) is expressed in neutrophils and displays cytotoxicity against Gram-negative bacteria. A recombinant fragment corresponding to the BPI N-terminus is currently in phase III clinical trials [8]. Other examples of AMPs resulting from proteolysis include cathelicidins from neutrophils [9] and cryptdins, α-defensins secreted by intestinal Paneth cells, whose bactericidal activity requires activation of a precursor by a metalloprotease [10].

We are currently working on ECP (eosinophil cationic protein) as a model of the potential involvement of mammalian RNases in the host defence system. ECP is a secretory ribonuclease (also known as RNase 3) found in the eosinophilic leucocyte and potentially involved in innate immunity. ECP can also be expressed at lower levels by activated neutrophils. Although the role of eosinophils during infection is controversial, eosinophils are activated, and selectively release their content, at the inflammation areas [11]. Some authors have reported antimicrobial activities for eosinophils and have proposed a complementary action, together with neutrophils, during bacterial infections [11]. Besides local protein secretion, which can harm the host tissues, eosinophils may also participate in immunoregulation and tissue remodelling processes [12,13]. Although a wealth of structural and functional data have been reported, the physiological role of ECP remains elusive [14]. Its cytotoxic activity is effective against a wide range of pathogens, suggesting a relatively non-specific mechanism of action. Although there is no evidence of direct *in vivo* involvement of ECP in the host response to bacterial infection, ECP kills both Gram-negative and Gram-positive strains at a low micromolar
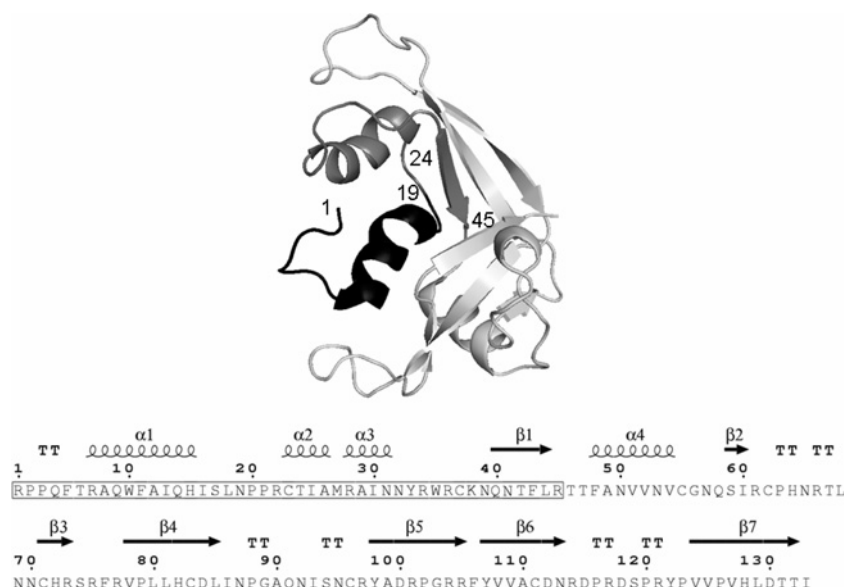
Figure 1   Graphical representation of the 3D structure of ECP

Drawn with PyMOL (DeLano Scientific; http://www.pymol.org). The ECP primary sequence and its secondary elements are drawn with ESPript. The main chains of regions 1–19, 24–45 and 1–45 are labelled in darker grey tones and the corresponding primary sequence is boxed.

range and its activity depends on its action both at the bacterial cell wall and cytoplasmic membrane levels [15–18]. ECP belongs to the vertebrate RNase A superfamily, of which several members are endowed with antimicrobial properties (see Supplementary Figure S1 available at http://www.BiochemJ.org/bj/421/bj4210425add.htm) [19–21]; the family that may have started off playing a physiological role in the host immune system [22–24]. Interestingly, ECP antibacterial activity is not shared by EDN (eosinophil-derived neurotoxin), a closely related eosinophil ribonuclease [25]. Antimicrobial RNases, as innate immune proteins with anti-infective and immunomodulatory properties, present substantial therapeutic potential in the drug development industry, both in the search for alternative antibiotics and for the treatment of inflammatory disorders.

In order to identify the structural determinants of ECP's cytotoxic mechanism of action, we have searched the ECP sequence for potential active domains using a theoretical approach to spot key antimicrobial regions (M. Torrent, V. Nogués and E. Boix, unpublished work), and have identified a potentially active region at the N-terminus. To validate our hypothesis, we have synthesized three peptides representative of this region (Figure 1) and assessed their properties both on a synthetic membrane model and on bacterial cell cultures.

EXPERIMENTAL

Materials

DOPC (dioleoyl phosphatidylcholine), DOPG (dioleoyl phosphatidylglycerol), (6,7)-Br$_2$PC, (9,10)-Br$_2$PC, and 11,12-Br$_2$PC [1-palmitoyl-2-stearoyl-(6,7, 9,10 and 11,12)-dibromo-*sn*-glycero-3-phosphocholine respectively] were from Avanti Polar Lipids. ANTS (8-aminonaphthalene-1,3,6-trisulfonic acid disodium salt) and DPX (*p*-xylenebispyridinium bromide) were from Invitrogen. Bovine pancreatic ribonuclease A, type XII-A, polymyxin B sulfate, LT (lipoteichoic acids) from *Staphylococcus aureus*, and LPS (lipopolysaccharides) from *Escherichia coli* serotype 0111:B4 were

purchased from Sigma–Aldrich. BC (BODIPY® TR cadaverine; where BODIPY® is boron dipyrromethane (4,4-difluoro-4-bora-3*a*,4*a*-diaza-*s*-indacene) and DiSC$_3$(5) (3,3 dipropylthiacarbocyanine) were purchased from Invitrogen. PD-10 desalting columns with Sephadex G-25 were from Amersham Pharmacia Biotech. *E. coli* BL21DE3 (Novagen) and *S. aureus* 502 A (ATCC) strains were used.

Peptides

Peptide ECP-(1–19) was obtained from NeoMPS. ECP-(24–45) and ECP-(1–45), with cysteine residues at positions 23 and 37 replaced by serine, were prepared by Fmoc (fluoren-9-ylmethoxycarbonyl) solid-phase peptide synthesis methods [26]. All peptides were purified by HPLC to ∼95 % homogeneity and were satisfactorily characterized by MALDI–TOF-MS (matrix-assisted laser-desorption ionization–time-of-flight MS). Further experimental details can be found in the Supplementary Experimental section and Figures S6–S8 available at http://www.BiochemJ.org/bj/421/bj4210425add.htm.

Expression and purification of ECP

Wild-type ECP was obtained from a human ECP synthetic gene [27]. Protein expression in the *E. coli* BL21DE3 strain, folding of the protein from inclusion bodies and the purification steps were carried out as described in [27].

IC$_{50}$ determination

Antimicrobial activity was expressed as the IC$_{50}$. The IC$_{50}$ of each peptide was determined from two independent experiments performed in triplicate for each peptide concentration. Peptides were dissolved in 10 mM sodium phosphate (Na$_2$HPO$_4$/NaH$_2$PO$_4$) buffer, pH 7.5, and serially diluted from 10 μM to 0.2 μM. Bacteria were incubated at 37 °C overnight in LB (Luria–Bertani) broth and diluted to give approximately 5 × 10^5 CFU (colony-forming units/ml. In each assay peptide solutions were added to each bacteria dilution, incubated for 4 h,

and samples were plated on Petri dishes and incubated at 37 °C overnight. The CFU in each Petri dish was counted, the average and the S.E.M. calculated and represented in a semi-logarithmic plot.

MIC (minimal inhibitory concentration) determination

Antimicrobial activity was expressed as the MIC, which is defined as the lowest concentration of peptides that completely inhibits microbial growth. MIC of each peptide was determined from two independent experiments performed in triplicate for each peptide concentration. Peptides were dissolved in 10 mM sodium phosphate buffer, pH 7.5 and serially diluted from 100 μM to 0.2 μM. Bacteria were incubated at 37 °C overnight in LB broth and diluted to give approximately 5×10^5 CFU/ml. In each assay peptide solutions were added to each bacteria dilution, incubated for 4 h and samples were plated on to Petri dishes and incubated at 37 °C overnight.

Liposome preparation

LUVs (large unilamellar vesicles) of a defined size (approx. 200 nm) were prepared from a vacuum-drying lipids chloroform solution by extrusion through 800, 400 and 200 nm polycarbonate membranes as described in [16]. The lipid suspension was frozen and thawed several times prior to extrusion. Liposomes containing DOPC/DOPG (3:2 molar ratio) were obtained. A 1 mM stock solution of liposome suspension in 10 mM Tris/HCl, pH 7.4, and 0.1 M NaCl was prepared.

Fluorescence measurements

Tryptophan fluorescence emission spectra were recorded using a 280 nm excitation wavelength. Slits were set at 2 nm for excitation and 5–10 nm for emission. Emission spectra were recorded from 300–400 nm at a scan rate of 60 nm/min, in a 10 mm × 10 mm cuvette with stirring immediately after sample mixing. Protein and peptide spectra at 0.5 μM in 10 mM Hepes buffer, pH 7.4, were obtained at 25 °C in the absence or presence of 200 μM liposome suspension, 200 μM LPS, assuming a 90 000 g/mol molecular mass, or 200 μM LTA, as calculated from a 2200 molecular mass reference value. Fluorescence measurements were performed on a Cary Eclipse spectrofluorimeter. Spectra in the presence of liposomes were corrected for light scattering by subtracting the corresponding LUV background. For each condition three spectra were averaged. The fluorescence spectra were also calculated as a function of the frequency scale (wave number) and adjusted using a log-normal function as detailed in [16].

Depth-dependent fluorescence quenching experiments using labelled brominated lipids

Quenching of protein tryptophan residues by brominated lipids was introduced to analyse the relative location of both Trp[10] and Trp[35] residues upon membrane interaction. LUVs of DOPC/DOPG (3:2 molar ratio) were prepared as described in [16], containing either (6,7)-, (9,10)-, or (11,12)-Br$_2$PC. Brominated lipids were mixed at increasing percentages, from 20 up to 80 %, with unlabelled DOPC/DOPG vesicles. The emission fluorescence spectra were recorded at 25 °C using the following conditions: 10 mM Tris/HCl buffer, pH 7.4, 0.5 μM protein concentration and 200 μM liposome concentration, excitation wavelength of 280 nm, with excitation and emission slits set to 2 nm and 10 nm respectively. For each condition three spectra were averaged. The

quenching efficiency of brominated lipids on protein tryptophan fluorescence was determined by calculating the area under the fluorescence spectra in range of 320 to 380 nm. Relative fluorescence intensities (F_0/F) were compared, where F_0 is the fluorescence intensity in the absence of quencher. To calculate the depth of insertion of the protein in the lipid bilayer the distribution analysis (DA) was employed, as detailed in [16].

ANTS/DPX liposome leakage assay

The ANTS/DPX liposome leakage fluorescence assay was performed as described in [16,28]. Briefly, a unique population of LUVs of DOPC/DOPG (3:2 molar ratio) lipids was obtained containing 12.5 mM ANTS, 45 mM DPX, 20 mM NaCl and 10 mM Tris/HCl, pH 7.5. The ANTS/DPX liposome suspension was diluted to 30 μM and was incubated at room temperature (25 °C) in the presence of ECP or the synthetic peptides. The leakage activity was assayed at different polypeptide concentrations, up to 8 μM, by following the release of the liposome content. Fluorescence was measured using a 386 nm excitation wavelength and 535 nm emission wavelength. Slits were set at 5 nm and 10 nm for excitation and emission respectively. The percentage of leakage (%L) produced by the proteins after 1 h of incubation with the liposomes was calculated with the following equation: $\%L = 100(Fp - F_0)/(F_{100} - F_0)$, where Fp is the final fluorescence intensity after addition of the protein (1 h), F_0 and F_{100} are the fluorescence intensities before addition of the protein and after addition of 0.5 % Triton X100. For each protein concentration three calculated leakage values were averaged. Leakage could not be quantified for those samples where the assay conditions triggered LUV precipitation, such as LUV samples incubated with high ECP protein concentrations.

LUV liposome aggregation

Aggregation of LUV lipid vesicles was monitored by measuring the scattering intensity with the excitation and emission wavelengths set at 470 nm using a Cary Eclypse spectrofluorimeter and cuvettes with an optical path of 1 cm. Prior to the addition of ECP and peptides, the vesicles were allowed to equilibrate for 15 min at room temperature. The buffer used was 10 mM Hepes, pH 7.4. Final assay conditions were 200 μM lipid and from 0.04 μM to 4 μM polypeptide range, in 10 mM Hepes buffer, pH 7.4. After 30 min of incubation at room temperature, the signal was read at 90° from the excitation beam with slits at 5 nm and 10 nm.

CD spectroscopy

The far-UV CD spectra were collected with a JASCO J-715 spectropolarimeter. Spectra were recorded from 250 nm up to 190 nm, at 1 nm intervals, 1 nm bandwidth, with a scan speed of 10 nm/min, at 25 °C. 0.2 cm pathlength cuvettes were used. Mean-residue ellipticity [θ] (deg · cm^2 · dmol^{-1}) was calculated using the formula:

$$[\theta] = \frac{\theta(\mathrm{MRW})}{10cl}$$

where MRW is the mean residue molecular mass of the protein, c is the protein concentration and l is the cell pathlength. Data of four consecutive scans were averaged and a linear smoothing from each five consecutive measurements was applied. ECP and peptides spectra in the absence and presence of SDS and LPS were recorded. ECP or peptide at 4–8 μM, diluted in 5 mM sodium phosphate buffer, pH 7.5, 1 mM SDS and 1 mM LPS

(assuming a 90 000 g/mol molecular mass), were used. Samples were centrifuged for 5 min at 10 000-**g** before use. For near-UV CD, spectra were recorded from 340 nm up to 255 nm, at 1 nm intervals, 1 nm bandwidth, with a scan speed of 10 nm/min, at 25 °C in 1 cm pathlength cuvettes. Data from four consecutive scans were averaged. ECP and peptides spectra in the absence and presence of LPS were recorded. ECP or peptide at 80–100 μM, diluted in 5 mM sodium phosphate buffer at pH 7.5, and 1 mM LPS (assuming a 90 000 g/mol molecular mass), were used. Percentage of each secondary structure was estimated using the JASCO software, based on the calculation method described by Yang et al. [29].

Bioinformatic analysis tools for peptide characterization

Physicochemical properties of peptides (pI and net charge) were predicted using the Swiss-Prot expasy server (http://www. expasy.ch/sprot/). Transmembrane-prediction domain analysis was performed using the Membrane Protein Explorer server (MPEx; http://blanco.biomol.uci.edu/mpex). Sequences with aggregation propensity were predicted using the Aggrescan server [30].

Bacterial cytoplasmic membrane depolarization assay

Membrane depolarization was monitored as described in [17], using the DiSC$_3$(5) lipophilic dye, which changes its fluorescence intensity in response to changes in transmembrane potential. *E. coli* and *S. aureus* cells were grown to mid-exponential phase and resuspended in 5 mM Hepes/KOH, 20 mM glucose, and 100 mM KCl at pH 7.2 to an attenuance (D_{600}) of ~0.05. DiSC$_3$(5) was added. Changes in the fluorescence due to the alteration of the cytoplasmic membrane potential were continuously monitored at 20 °C by fluorescence emission at 670 nm using an excitation wavelength of 620 nm. When the dye uptake was maximal, as indicated by a stable reduction in the fluorescence because of quenching of the accumulated dye at the membrane, polypeptide samples were added at a final concentration of 4 μM. All conditions were assayed in duplicate. The time necessary to reach a stabilized maximum fluorescence reading was recorded for each condition.

Fluorescent probe displacement assay for lipolysaccharide binding

LPS binding was assessed using the fluorescent probe BC as described in [17]. BC binds strongly to native LPS, specifically recognizing the lipid A portion. LPS-binding assays were carried out in 5 mM Hepes buffer, pH 7.5. The displacement assay was performed by the addition of 1–2 μl aliquots of a stock solution of ECP and peptides to 1 ml of a continuously stirred mixture of LPS at 10 μg/ml and BC (10 μM). The BC excitation wavelength was 580 nm and emission wavelength was 620 nm. Excitation and emission slits were set at 2.5 nm and 20 nm respectively. Final values correspond to an average of four replicates. Quantitative effective displacement values (ED$_{50}$) were calculated. The ED$_{50}$ was computed at the midpoint of the fluorescent signal against the protein concentration of the displacement curve by a curve-fitting of the data to the equation:

$$OF = \frac{F_0 - F}{F_0 - F_{max}}$$

where *OF* is the occupancy factor, F_0 the fluorescence intensity of BC alone, F_{max} is the intensity in the presence of LPS at saturation concentration and F is the intensities of the LPS/BC mixtures at each displacer concentration. Polymyxin B and RNase A were used as positive and negative controls respectively.

SEM (Scanning electron microscopy)

Cultures of *E. coli* and *S. aureus* (1 ml) were grown at 37 °C to mid-exponential phase (D_{600} ~ 0.4) and incubated with 10 μM ECP and the derived peptides in PBS at room temperature. Sample aliquots (500 μl) were taken after up to 4 h of incubation and prepared for SEM analysis as described in [17]. The micrographs were viewed at a 15 kV accelerating voltage on a Hitachi S-570 scanning electron microscope, and a secondary electron image of the cells for topography contrast was collected at several magnifications.

TEM (Transmission electron microscopy)

Mid-logarithmic phase *E. coli* and *S. aureus* cells (D_{600} ~ 0.4) were incubated with 10 μM ECP and peptides for 4 h. After treatment, bacterial pellets were pre-fixed with 2.5 % (w/v) glutaraldehyde and 2 % (w/v) paraformaldehyde in 0.1 M sodium cacodylate buffer, pH 7.4, for 2 h at 4 °C, and post-fixed in 1 % (w/v) osmium tetroxide in 0.1 M sodium cacodylate buffer, pH 7.4, for 2 h at 4 °C. The samples were dehydrated in acetone (50, 70, 90, 95 and 100 %). The cells were immersed in EPON (liquid epoxy) resin, and ultrathin sections were examined on a JEOL JEM 2011 microscope.

RESULTS

Antimicrobial activity

Sequence analysis of ECP suggests that the N-terminus might contain an antimicrobial domain. Applying a predictive strategy based on previous high-throughput peptide library screening results [31], a bactericidal propensity value was assigned to each amino acid (M. Torrent, V. Nogués and E. Boix, unpublished work). On ECP a main potential active region at the N-terminus (residues 30–45) was identified. To test the activity of this region of ECP, the full N-terminal domain, ECP-(1–45), as well as two smaller representative peptides, ECP-(1–19) and ECP-(24–45), were chosen for the present study (Figure 1). ECP-(1–45) includes the first ECP α-helix elements (α1, α2 and α3) and the first β-region (β1). The ECP-(24–45) peptide spans the main predicted sequence and includes the Trp[35]–Arg[36] residues previously identified as the determinant for cytotoxicity and membrane lysis activity [16,28,32]. The ECP-(1–19) peptide, which corresponds to the first α1 domain, represents the ECP homologue of the S-peptide in RNase A [33].

The bactericidal properties of the three peptides against two representative Gram-negative and -positive strains (*E. coli* and *S. aureus* respectively) have been compared with those of the full ECP sequence. Analysis of the IC$_{50}$ and the MIC values (Table 1) shows the ECP-(1–45) segment to be practically equivalent to the entire native sequence in terms of antimicrobial activity against both strains. Within the ECP-(1–45) segment, activity is shown to be mostly confined to residues ECP-(24–45), whereas the ECP-(1–19) peptide requires approx. 10–20-fold higher concentrations to display significant bactericidal activity. As shown in Table 1, ECP and the three tested peptides displayed similar active ranges against both *E. coli* and *S. aureus*.

The bactericidal effects of the peptides on either strain have been further analysed to better characterize their distinct properties. ECP can depolarize the cytoplasmic membrane of both *E. coli* and *S. aureus* cells [17]. The evaluation of the protein capacity to depolarize the bacteria cytoplasmic cell is an indirect method to assess its ability to interact at the bacteria surface and alter the inner membrane. Previous results on ECP depolarization capacity indicated that its activity is higher in

Table 1   IC$_{50}$ and MIC of ECP and peptides

Bacteria were incubated at 37°C overnight in LB and diluted to give approx. 5×10^5 CFU/ml. Final values were determined from two independent experiments performed in triplicate for each peptide concentration. IC$_{50}$ values are means $\pm$ S.E.M.

Polypeptide	Bactericidal activity (*E. coli*)		Bactericidal activity (*S. aureus*)	
	IC$_{50}$ (μM)	MIC (μM)	IC$_{50}$ (μM)	MIC (μM)
ECP	0.045 $\pm$ 0.007	0.30–0.50	0.045 $\pm$ 0.004	0.30–0.50
ECP-(1–45)	0.058 $\pm$ 0.009	0.5–0.75	0.060 $\pm$ 0.004	0.50–0.75
ECP-(24–45)	0.282 $\pm$ 0.010	5–10	0.173 $\pm$ 0.002	1.00–2.00
ECP-(1–19)	2.866 $\pm$ 0.053	50–100	3.579 $\pm$ 2.452	50–100
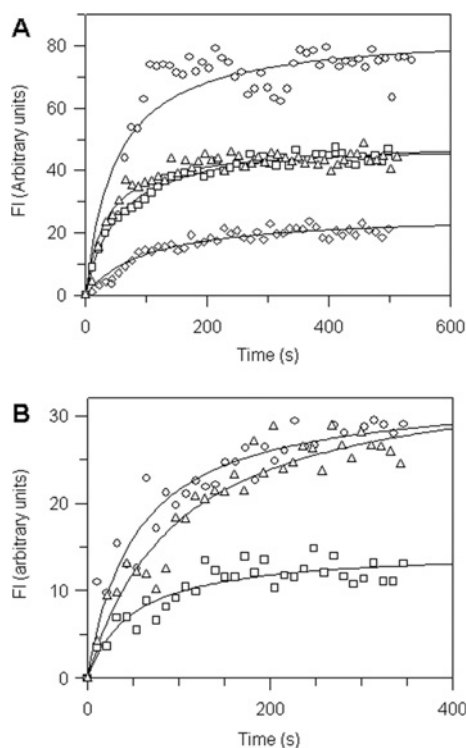
Figure 2   Depolarization activity on *E. coli* and *S. aureus* cells determined by the DiSC$_3$(5) dye assay

(**A**) *E. coli*. (**B**) *S. aureus*. Bacterial cells were grown at 37°C to mid-exponential phase ($D_{600} = 0.4$), and resuspended in 5 mM Hepes/KOH, 20 mM glucose and 100 mM KCl, pH 7.2, to D_{600} of $\sim$0.05. DiSC$_3$(5) was added and, when the dye uptake was maximal, polypeptides in 5 mM Hepes/KOH buffer, pH 7.2, were added at a final concentration of 4 μM. The increase in fluorescence intensity (FI) registers the dye release upon reduction of the transmembrane potential. ECP, (○); ECP-(1–45), (△); ECP-(24–45), (□); and ECP-(1–19), (◇). No activity was registered for *S. aureus* cells incubated with ECP-(1–19).

the Gram-negative-tested strain, probably as a consequence of the easier access of the protein to the cytoplasmic membrane [17]. In fact, ECP can alter by itself the Gram-negative strain outer membrane structure [17]. We compared the protein depolarization capacity with the corresponding N-terminal peptides (Figure 2). ECP-(1–45) is the most active segment, whereas ECP-(24–45) retains an intermediate activity and ECP-(1–19) shows the worst performance, as previously observed for the corresponding bactericidal values (Table 1). However, significant differences between the two strains of bacteria are found. Whereas in *E. coli* ECP-(1–45) and ECP-(24–45) both have intermediate activity and ECP-(1–19) is quite inactive, in *S. aureus* ECP-(1–45) is nearly equipotent with ECP, and ECP-(1–19) is totally inactive.
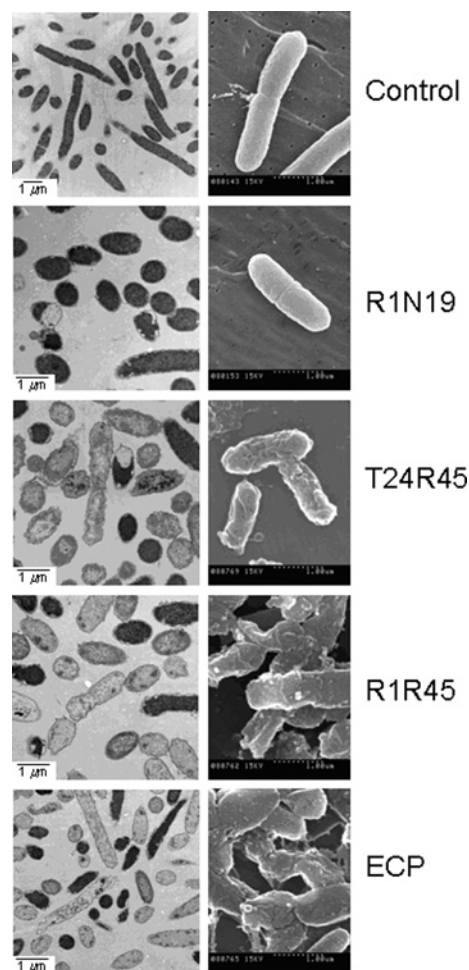
Figure 3   TEM and SEM of *E. coli* incubated with ECP or ECP-derived peptides

Left-hand panel, TEM. Right-hand panel, SEM. Each sample was incubated with 10 μM of ECP or ECP peptides for 3 h. From top to bottom: control cells; ECP-(1–19), R1N19; ECP-(24–45), T24R45; ECP-(1–45), R1R45; and ECP.

For a better understanding of the cytotoxic activities of the peptides on bacteria we analysed their effects by electron microscopy. Potential damage on both the bacteria wall surface and the cytoplasmic membrane can be visualized by TEM. In *E. coli*, ECP promotes outer membrane detachment, alteration of the overall cell shape and partial loss of cell content [17]. Comparison of the peptides with ECP confirms that both ECP-(1–45) and ECP-(24–45) are very active against *E. coli* (Figure 3). TEM micrographs include many hypodense damaged cells with vacuolization, local outer membrane detachment and loss of characteristic baton-shaped morphology. In contrast, practically no damaged cells can be seen upon treatment with ECP-(1–19). For *S. aureus* (see Supplementary Figure S2 available at http://www.BiochemJ. org/bj/421/bj4210425add.htm), TEM micrographs also show some hypodense cells for ECP-(1–45) and ECP-(24–45), although the overall damage is comparatively much less for this strain. ECP-(1–45) relative damage is similar to ECP, while ECP-(24–45) is slightly less active. As above, no significant effect is visible for ECP-(1–19).

Complementary analysis by SEM further illustrated the effect of the peptides on the bacterial surface. For ECP, previous data

Table 2 Maximum position of intrinsic fluorescence spectra of polypeptides in the absence and presence of liposomes, LPS and LTA

Fluorescent emission spectra were recorded from 300 nm to 400 nm using a 280 nm excitation wavelength. The data were fitted with a log-normal function as described in [16]. Quantitative effective displacement values (ED_{50}) for LPS binding, calculated from curves in Supplementary Figure S3 (see http://www.BiochemJ.org/bj/421/bj4210425add.htm), are also included. N.D., no displacement is detected.

Polypeptide	Control λ_{max} (nm)	DOPC/DOPG (3:2) λ_{max} (nm)	λ shift (nm)	LPS λ_{max} (nm)	λ shift (nm)	LTA λ_{max} (nm)	λ shift (nm)	LPS binding ED_{50} (μM)
ECP	344	339	5	340	4	340	4	0.080 $\pm$ 0.001
ECP-(1–45)	352	342	10	344	8	342	10	0.780 $\pm$ 0.001
ECP-(24–45)	355	341	14	346	9	344	11	1.525 $\pm$ 0.004
ECP-(1–19)	339	336	3	337	2	337	2	N.D.

indicated a high ability to aggregate *E. coli* cells and to damage their wall envelope [17]. This cell agglutination ability is retained by ECP-(1–45) (Figure 3), whereas no aggregates are observed upon incubation with the shorter peptides ECP-(24–45) and ECP-(1–19). On the other hand, significant surface wall damage is evident for cells treated with both ECP-(1–45) and ECP-(24–45), whereas little effect is seen upon incubation with ECP-(1–19). SEM micrographs of ECP-treated *S. aureus* cells did not reveal any aggregate, as reported previously [17]. Surface wall damage for *S. aureus* cells is only mild compared with the treated *E. coli* cells but some local blebs appear. Cells incubated with ECP-(1–45) show nearly the same pattern, with ECP-(24–45) wall damage is quite mild and with ECP-(1–19) it is undetectable (see Figure S2).

Outer membrane detachment, visualized by electron microscopy, is considered to be related to an uncommonly high ability of ECP to bind LPS, the main component of Gram-negative bacterial surfaces, and its antigenic portion, the lipid A [17]. We compared the LPS binding capacity of ECP and its N-terminal fragments. A decreasing order of LPS binding abilities, from ECP-(1–45) to ECP-(1–19), is registered (Table 2, and see Supplementary Figure S3 available at http://www.BiochemJ.org/bj/421/bj4210425add.htm). The displacement ability of ECP-(1–45) is considerably lower than that of ECP, but still high if compared with the positive control polymyxin B (Figure S3). On the other hand, ECP-(1–19) does not have any significant affinity to LPS. The LPS binding process can also be followed by the analysis of the intrinsic fluorescence spectra (Table 2). The recorded blue-shifts suggest that tryptophan residues are involved in the interaction and that Trp[35] might be the residue that alters its environment most upon binding. Whereas the native protein does not modify its overall structure upon LPS binding, as assessed by CD spectra, we observe significant changes for the peptides, with an increase in their secondary structure content (see Figure 6). The near-UV spectra indicate that changes in the local environments of the aromatic residues take place in the presence of LPS. A careful inspection reveals that ECP-(1–19) does not significantly modify its overall profile, but that both ECP-(1–45) and ECP-(24–45) register an altered profile. In particular, ECP-(1–45) drastically shifts the bands in the characteristic ranges for tyrosine and tryptophan, suggesting the involvement of the exposed Tyr[33] and Trp[35] residues in LPS binding. Interestingly, both ECP-(1–45) and ECP-(24–45) peptide far-UV spectra in the presence of LPS indicate a much more structured conformation upon binding (see Figure 6).

Additionally, in order to identify potential interactions between the protein and the N-terminal peptides at the Gram-positive bacteria surface, we have also analysed the changes in the intrinsic fluorescence spectra in the presence of LTA. Electrostatic interactions between the polypeptide cationic residues and the negative-charged groups of LTA are expected. Results confirmed the binding of LTA and the contribution of tryptophan residues (Table 2). Pronounced shifts are mainly recorded for ECP-(1–45) and ECP-(24–45) peptides, with comparable values, whereas the blue-shift corresponding to ECP-(1–19) is only minor, suggesting the involvement of Trp[35] in the interaction.

Interaction with lipid bilayers

The correlation between ECP cytotoxic activity and its membrane-destabilizing capacity has been previously reported [28,32]. Detailed analysis of ECP action using LUV and giant unilamellar vesicles as membrane models revealed aggregation and leakage activities in the nanomolar range [16,18]. In the present study, we characterized the interaction of ECP N-terminal peptides with LUV made up of DOPC/DOPG phospholipids.

The intrinsic fluorescence signals of the peptides were first analysed. ECP includes two tryptophan residues, Trp[10] and Trp[35], both present in the ECP peptides analysed, which have been classified into different spectral classes [34]. Comparison of ECP with single tryptophan mutants indicates that most of the blue-shift in the fluorescence spectrum is due to the association of solvent-exposed Trp[35] with the lipid bilayer [16]. The intrinsic fluorescence spectra of the peptides (see Supplementary Figure S4 available at http://www.BiochemJ.org/bj/421/bj4210425add.htm) indicate that, as expected, both tryptophan residues are far more highly solvent-exposed than in their respective locations within full-length ECP. Of the two, Trp[10] is the residue experiencing a more pronounced change, from a buried location in ECP [16] to a more exposed position in ECP-(1–19).

When the peptide spectra are recorded in the presence of the DOPC/DOPG LUV, a significant blue-shift is observed in all cases, confirming the interaction with the lipid bilayer. Shifts for ECP-(24–45) and ECP-(1–45) are more pronounced than for ECP-(1–19), suggesting that Trp[35] does undergo a more pronounced change on its microenvironment when the peptides associate with lipid bilayers. In fact, the similarity between spectra of ECP-(24–45) and ECP-(1–45) suggests that the Trp[10] contribution to the final signal is minor.

The interaction with lipid bilayers has been further investigated by fluorescence quenching experiments using brominated phospholipids. For that purpose, LUV made up of DOPC/DOPG with PC dibromo derivates at several positions remote from the head group (6,7, 9,10 and 11,12 respectively) have been prepared. This methodology allows an estimation of the degree of peptide insertion into the lipid bilayers. The quenching efficiency of the differently brominated lipids has been recorded by comparing the respective fluorescence quenching slopes. For all peptides, the presence of either Trp[10] or Trp[35] allowed the
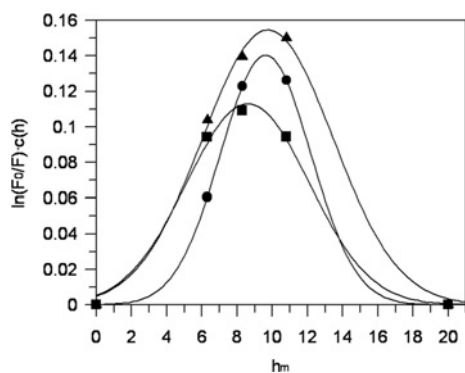
Figure 4   Depth-dependent fluorescence quenching profiles calculated by distribution analysis to visualize changes in the tryptophan chromophore (F) fluorescence, normalized to its value in the absence of quenching (F_0), when the quencher is present at certain depths in the bilayer

h_m is the average location depth of the tryptophan residues, calculated from the bilayer centre. Liposomes containing DOPC/DOPG (3:2) were mixed with increasing molar ratios of (6,7)-, (9,10)-, or (11,12)-Br$_2$PC. Assay conditions were 0.5 μM final protein concentration and 200 μM liposome concentration. ECP-(1–19), (■); ECP-(24–45), (▲); and ECP-(1–45), (●).

monitoring of changes upon membrane interaction. The Stern–Volmer quenching slopes show a steep decrease from the 6,7- to the 11,12-dibrominated LUV, indicating a diminishing interaction between the tryptophan residues and the bromine-labelled phospholipid (see Supplementary Figure S5 available at http://www.BiochemJ.org/bj/421/bj4210425add.htm). From these results an average insertion of ~ 10 Å (1 Å = 0.1 nm), from the bilayer centre, can be estimated for the tryptophan residues of both ECP-(24–45) and ECP-(1–45), similar to that in ECP [16], while a slightly deeper insertion (~ 8 Å) is found for the ECP-(1–19) peptide (Figure 4).

Another way to evaluate lipid bilayer destabilization is by determining the ability to aggregate LUV, triggering leakage and release of vesicles' aqueous content. Thus ECP promotes the release of encapsuled ANTS/DPX at a 1:300 protein/lipid ratio and above [16]. Consistent with these trends, the leakage ability of ECP-(1–45) is similar to ECP, that of ECP-(24–45) is slightly lower, whereas ECP-(1–19) requires much higher peptide/lipid ratios to induce significant leakage (Figure 5A).

Liposome aggregation can also be monitored by the increase in scattering intensity at 470 nm. Using this method, ECP has detectable LUV aggregation above a 1:1500 protein/lipid molar ratio [16], which is mostly retained by ECP-(1–45) but, surprisingly, lost in the ECP-(24–45), whereas partial aggregating behaviour is observed for ECP-(1–19) (Figure 5B).

Finally, we have used CD to investigate the conformational changes brought about by peptide–membrane interaction (Figure 6). The CD spectrum of ECP in aqueous solution has been reported [35], with the inferred secondary structure values showing some deviation from those derived from X-ray crystallography [36]. These differences were mainly attributed to the contribution of aromatic amino acid side chains to the spectral profile. Comparison of the near-UV spectra of ECP and the peptides (Figure 6), reveals significant changes in local environment for aromatic residues in ECP-(1–45) and ECP-(24–45).

We have also analysed the far-UV spectra for ECP and the derived peptides in the absence and presence of SDS (Figure 6). The results for ECP indicate that no overall conformation changes have taken place (Figure 6A). In contrast, for the three peptides some significant differences were observed (Figures 6B–6D). SDS induced the transition to more structured conformations for the three peptides, where a reduction in the β-sheet content
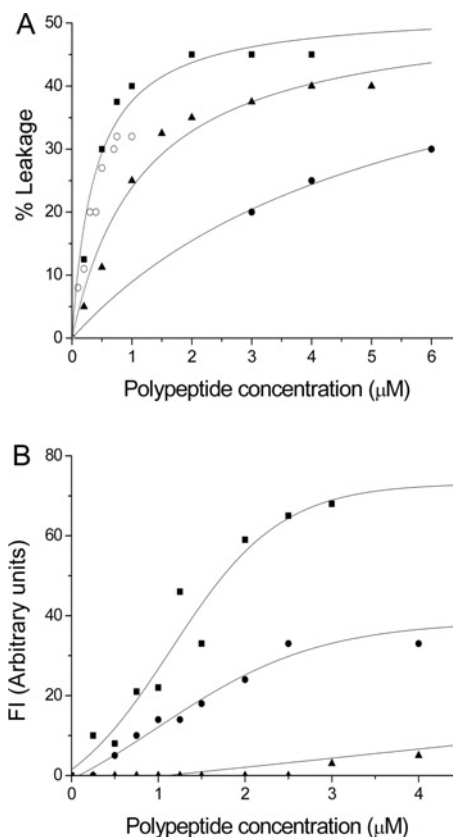

Figure 5   ECP peptide action on lipid bilayers

(**A**) Leakage activity was monitored by release of ANTS/DPX liposome content. Percentage of leakage (% Leakage) produced by the polypeptides after 1 h incubation with liposomes at room temperature is shown. (**B**) LUV aggregation as a function of polypeptide concentration. LUVs were incubated with each peptide and aggregation was monitored as an increase in scattering intensity at 470 nm at 90° from the excitation beam, after 30 min of incubation at room temperature. ECP, (○); ECP-(1–45), (■); and ECP-(24–45), (▲); and ECP-(1–19), (●).

and a significant increase in the α-helical content is registered. Thus we can conclude that when exposed to a lipid environment the peptides undergo conformational reorganization, with a considerable increase in their structured content. Comparison of the α-helix content for each peptide indicates an increase of 25, 35 and 70 % for ECP-(1–19), ECP-(24–45) and ECP-(1–45) respectively. This is consistent with their respective abilities to disrupt lipid bilayers (Figure 5A). On the other hand, prediction of potential transmembrane segments using the MPEx software identifies a segment from residues 9 to 27 with a high tendency to form an α-helix in a lipid environment. This might explain why the peptide with the highest activity on lipid bilayers is ECP-(1–45), which includes this segment in its entirety.

DISCUSSION

ECP is an eosinophil-secreted protein involved in inflammation processes with diverse antipathogen properties [14,37]. In previous studies we have characterized its bactericidal activity and identified some structural determinants for its cytotoxic capacity [16–18,28]. ECP diverged from the other eosinophil RNase, EDN, under an unusual evolutive pressure and acquired a higher cationicity and cytotoxicity [38]. We have now identified an N-terminal region that retains both the bactericidal and membrane-disrupting activities of ECP. The selected 1–45
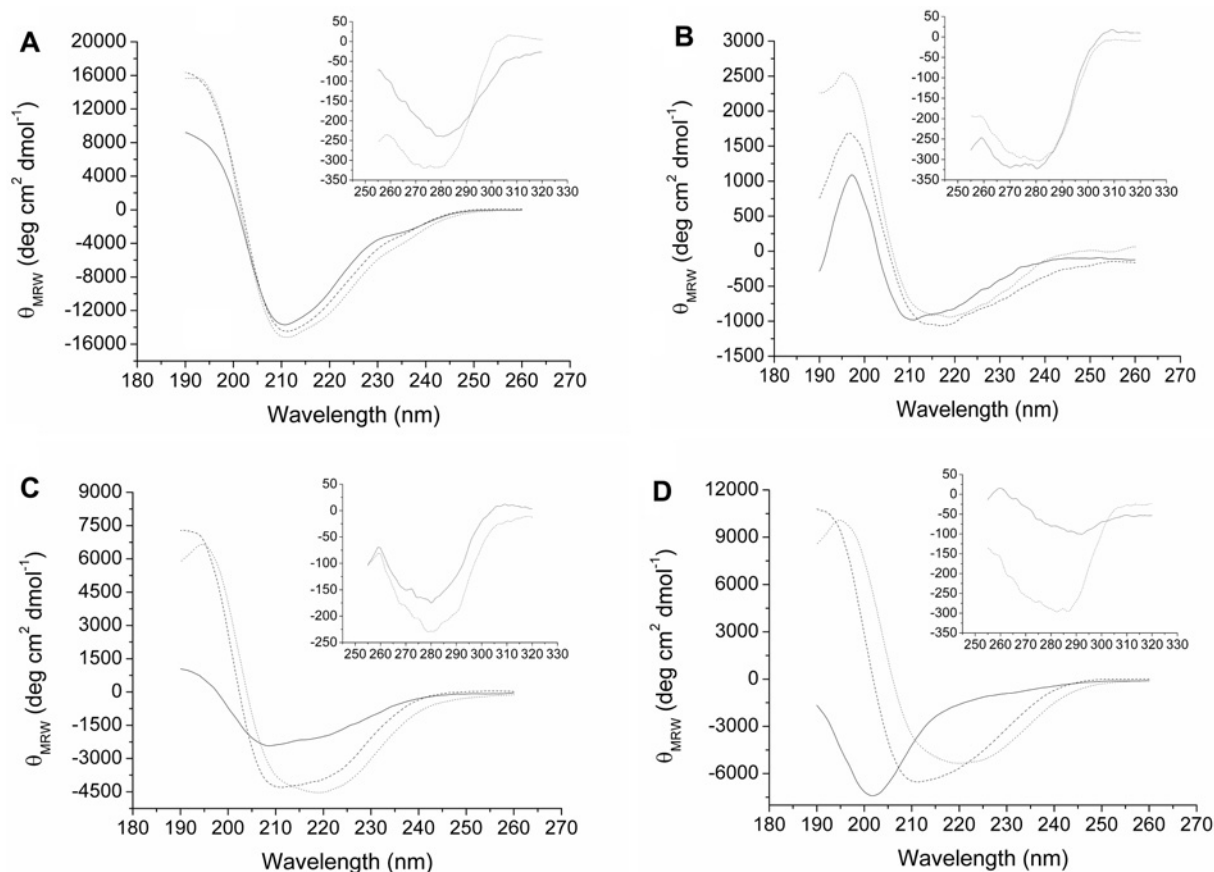
Figure 6   CD far-UV spectra of ECP and derived ECP peptides in the absence and presence of SDS and LPS

(**A**) ECP. (**B**) ECP-(1–19). (**C**) ECP-(24–45). (**D**) ECP-(1–45). Absence of SDS (solid line), presence of SDS (· · · · ·) and presence of LPS (- - - - -). Results are the average of four consecutive scans. Mean-residue ellipticity [θ] (deg · cm^2 · dmol^{-1}) was calculated. Insets: the CD near-UV spectra in the absence (solid line) and presence (- - - -) of LPS.

segment fulfils the common structural and chemical criteria for AMPs [1,39,40]. It includes a high number of arginine residues, which confer the three synthetic peptides with a net positive charge [+2, +5 and +8 for ECP-(1–19), ECP-(24–45) and ECP-(1–45) respectively] as well as a high pI (predicted as 12, 11.5 and 11.9). On the other hand, the studied N-terminus includes two cysteine residues, which were substituted in the synthetic peptides by serine to avoid potential formation of intra- or inter-molecular disulfide bridges. Although the peptides cannot reproduce this full scenario (i.e. the context of the disulfide-bonded protein structure) the use of synthetic peptides with cysteine substitutions or deletions is a useful approach, as reported for other antimicrobial proteins [41]. In fact, some antimicrobial proteins do retain activity in their denatured state [6]. Furthermore, there is also a report of an antimicrobial RNase A homologue, the salmon RNase, which preserves activity when fully denatured [20]. Moreover, the characterization of protein-derived peptides was also successfully applied to avian leucocyte RNase A homologues (see Figure 1S), where one of the peptides outside the protein scaffold retained bactericidal activity [42]. A cationic cluster at the N-terminus was also identified for the skin-derived RNase 7, another human RNase A homologue (see Supplementary Figure S1) that contributes to the innate immunity at the skin–chemical barrier [43,44].

Comparison of the bactericidal and membrane-destabilizing activities of ECP and the three synthetic peptides indicates that the ECP N-terminus retains some sequence determinants involved at the different levels of ECP's cytotoxic capacity. The longest,

ECP-(1–45), displays nearly all of the bactericidal activity of the whole protein against *E. coli* and *S. aureus* strains, and partially retains the LPS binding and depolarization abilities. Additionally, ECP-(1–45) has almost the same membrane interaction capacity as ECP, with nearly equivalent leakage and liposome aggregation activities. The inner ECP-(24–45) peptide can partially, but not fully, reproduce the bactericidal and membrane destabilization capacities of the intact protein, and the short ECP-(1–19) peptide has almost no toxicity for bacterial cells.

Altogether, the results obtained reveal, once again, that membrane disruption cannot by itself explain the toxicity of ECP towards bacterial cells. Furthermore, the observed differences in the activity of ECP against Gram-negative and Gram-positive strains also suggest the involvement of strain-specific determinants in the killing events. Electron microscopy illustrates diverse abilities of the peptides at the bacterial wall surface. Similar bactericidal activities do not readily translate to bacteria wall damage, suggesting that cell viability is lost before any cell surface destruction is visualized. Although ECP and its derived peptides are bactericidal against both *E. coli* and *S. aureus*, bacterial wall damage is much more pronounced in the Gram-negative strain. ECP shows a specific capacity to destroy the *E. coli* outer membrane and to agglutinate the cells [17], and this ability is only retained by the full ECP-(1–45) fragment.

The propensity of ECP and its derived peptides to bind lipid bilayers may also be facilitated by their hydrophobicity and aggregation tendency. We used the Aggrescan software [30] to screen the ECP sequence for the presence of hydrophobic patches

that can favour aggregation. One such sequence is found at the ECP N-terminus (residues 8–16), and is not present in EDN. An N-terminal aggregation domain has also been identified in the skin-derived RNase 7, although not in other screened human RNases (results not shown). An exposed hydrophobic patch may promote both protein–protein and also protein–lipid bilayer interactions. The fact that ECP-(1–19) partially retains a lipid aggregation ability, whereas the internal segment ECP-(24–45) does not, also supports the presence of a potential 'aggregation-promoting' domain at the ECP N-terminus.

The short peptide ECP-(24–45) seems to include a key region for bactericidal action, as well as for specific binding to the bacteria wall. Both ECP-(1–45) and ECP-(24–45) retain part of ECP's affinity for LPS, with Tyr^{33} and Trp^{35} residues that might participate in the interaction. Recent results on the ECP–heparin binding affinity indicate that charged and aromatic residues 34–38 are involved in this selective ability [45], identifying a key domain responsible for protein anchoring to the cell surface. Recent work by Döring and co-workers [46] on the tyrosine nitration process activated during eosinophil maturation, identified in ECP a unique tyrosine nitration at residue 33 in ECP, and suggested that tyrosine nitration may modulate ECP aggregation and/or its interaction with other eosinophil proteins.

In view of all of the above results, we suggest that residues 1–45 of ECP embrace the main functional domain of the protein. In the present study we have shown that the ECP-(1–45) peptide reproduces most of ECP's antimicrobial properties. The inner ECP-(24–45) sequence retains the key bactericidal region, but loses some of ECP's membrane-destabilizing capacities. One can plausibly propose that the first 19 residues are also necessary either for preserving native-like conformation or for promoting aggregation, or both. Although devoid of significant bactericidal action, this 1–19 region retains membrane-destabilizing properties, consistent with data suggesting that it includes an aggregation patch.

In any event, ECP-derived peptides are one model of novel sources of AMPs as alternative antibiotics against resistant strains. The ECP *E. coli* cells agglutinating activity is indeed a promising property that is being investigated in the search for alternative antibiotics as a mechanism to induce bacteria clearance by the host phagocytic cells [47]. Given the pharmaceutical interest in the development of new LPS-binding substances for treatment of immune disorders, the partial LPS-binding ability in residues 24–45 also offers a starting template for the design of new peptide-derived immunomodulator drugs.

AUTHOR CONTRIBUTION

Marc Torrent carried out all the functional and structural characterization of the peptides, prepared all the corresponding artwork and actively participated in the methodology development, experiment setup and discussion and interpretation of results. David Andreu contributed to the peptides' design and final writing of the manuscript. Beatriz de la Torre synthesized the peptides. Victòria Nogués contributed to the paper's discussion and correction. Ester Boix conceived the experimental setup and drafted the manuscript. All authors read and approved to the final manuscript.

ACKNOWLEDGEMENTS

FUNDING

REFERENCES

1 Powers, J. P. and Hancock, R. E. (2003) The relationship between peptide structure and antibacterial activity. Peptides **24**, 1681–1691
2 Lohner, K. and Blondelle, S. E. (2005) Molecular mechanisms of membrane perturbation by antimicrobial peptides and the use of biophysical studies in the design of novel peptide antibiotics. Comb. Chem. High Throughput Screen. **8**, 241–256
3 Rivas, L., Luque-Ortega, J. R. and Andreu, D. (2009) Amphibian antimicrobial peptides and protozoa: lessons from parasites. Biochim. Biophys. Acta **1788**, 1570–1581
4 Hancock, R. E. and Sahl, H. G. (2006) Antimicrobial and host-defense peptides as new anti-infective therapeutic strategies. Nat. Biotechnol. **24**, 1551–1557
5 Gudmundsson, G. H. and Agerberth, B. (1999) Neutrophil antibacterial peptides, multifunctional effector molecules in the mammalian immune system. J. Immunol. Methods **232**, 45–54
6 During, K., Porsch, P., Mahn, A., Brinkmann, O. and Gieffers, W. (1999) The non-enzymatic microbicidal activity of lysozymes. FEBS Lett. **449**, 93–100
7 Nibbering, P. H., Ravensbergen, E., Welling, M. M., van Berkel, L. A., van Berkel, P. H., Pauwels, E. K. and Nuijens, J. H. (2001) Human lactoferrin and peptides derived from its N terminus are highly effective against infections with antibiotic-resistant bacteria. Infect. Immun. **69**, 1469–1476
8 Canny, G. and Levy, O. (2008) Bactericidal/permeability-increasing protein (BPI) and BPI homologs at mucosal sites. Trends Immunol. **29**, 541–547
9 Zanetti, M., Gennaro, R. and Romeo, D. (1995) Cathelicidins: a novel protein family with a common proregion and a variable C-terminal antimicrobial domain. FEBS Lett. **374**, 1–5
10 Ayabe, T., Satchell, D. P., Pesendorfer, P., Tanabe, H., Wilson, C. L., Hagen, S. J. and Ouellette, A. J. (2002) Activation of Paneth cell α-defensins in mouse small intestine. J. Biol. Chem. **277**, 5219–5228
11 Hogan, S. P., Rosenberg, H. F., Moqbel, R., Phipps, S., Foster, P. S., Lacy, P., Kay, A. B. and Rothenberg, M. E. (2008) Eosinophils: biological properties and role in health and disease. Clin. Exp. Allergy **38**, 709–750
12 Zagai, U., Skold, C. M., Trulson, A., Venge, P. and Lundahl, J. (2004) The effect of eosinophils on collagen gel contraction and implications for tissue remodelling. Clin. Exp. Immunol. **135**, 427–433
13 Gomes, I., Mathur, S. K., Espenshade, B. M., Mori, Y., Varga, J. and Ackerman, S. J. (2005) Eosinophil-fibroblast interactions induce fibroblast IL-6 secretion and extracellular matrix gene expression: implications in fibrogenesis. J. Allergy Clin. Immunol. **116**, 796–804
14 Boix, E., Torrent, M., Sánchez, D. and Nogués, M. V. (2008) The antipathogen activities of eosinophil cationic protein. Curr. Pharm. Biotech. **9**, 141–152
15 Lehrer, R. I., Szklarek, D., Barton, A., Ganz, T., Hamann, K. J. and Gleich, G. J. (1989) Antibacterial properties of eosinophil major basic protein and eosinophil cationic protein. J. Immunol. **142**, 4428–4434
16 Torrent, M., Cuyas, E., Carreras, E., Navarro, S., Lopez, O., de la Maza, A., Nogues, M. V., Reshetnyak, Y. K. and Boix, E. (2007) Topography studies on the membrane interaction mechanism of the eosinophil cationic protein. Biochemistry **46**, 720–733
17 Torrent, M., Navarro, S., Moussaoui, M., Nogués, M. V. and Boix, E. (2008) Eosinophil cationic protein high-affinity binding to bacteria-wall lipopolysaccharides and peptidoglycans. Biochemistry **47**, 3544–3555
18 Torrent, M., Sánchez, D., Buzón, V., Nogués, M.V., Cladera, J. and Boix, E. (2009) Comparison of the membrane interaction mechanism of two antimicrobial RNases: RNase 3/ECP and RNase 7. Biochim. Biophys. Acta **1788**, 1116–1125
19 Boix, E. and Nogues, M. V. (2007) Mammalian antimicrobial proteins and peptides: overview on the RNase A superfamily members involved in innate host defence. Mol. Biosyst. **3**, 317–335
20 Pizzo, E., Varcamonti, M., Di Maro, A., Zanfardino, A., Giancola, C. and D'Alessio, G. (2008) Ribonucleases with angiogenic and bactericidal activities from the Atlantic salmon. FEBS J. **275**, 1283–1295
21 Hooper, L. V., Stappenbeck, T. S., Hong, C. V. and Gordon, J. I. (2003) Angiogenins: a new class of microbicidal proteins involved in innate immunity. Nat. Immunol. **4**, 269–273
22 Cho, S. and Zhang, J. (2007) Zebrafish ribonucleases are bactericidal: implications for the origin of the vertebrate RNase A superfamily. Mol. Biol. Evol. **24**, 1259–1268

23 Rosenberg, H. F. (2008) RNase A ribonucleases and host defense: an evolving story. J. Leukocyte Biol. **83**, 1079–1087

24 Pizzo, E. and D'Alessio, G. (2007) The success of the RNase scaffold in the advance of biosciences and in evolution. Gene **406**, 8–12

25 Rosenberg, H. F. (2008) Eosinophil-derived neurotoxin/ RNase 2: connecting the past, the present and the future. Curr. Pharm. Biotech. **9**, 135–140

26 Fields, G. B. and Noble, R. L. (1990) Solid phase peptide synthesis utilizing 9-fluorenylmethoxycarbonyl amino acids. Int. J. Pept. Protein Res. **35**, 161–214

27 Boix, E., Nikolovski, Z., Moiseyev, G. P., Rosenberg, H. F., Cuchillo, C. M. and Nogues, M. V. (1999) Kinetic and product distribution analysis of human eosinophil cationic protein indicates a subsite arrangement that favors exonuclease-type activity. J. Biol. Chem. **274**, 15605–15614

28 Carreras, E., Boix, E., Rosenberg, H. F., Cuchillo, C. M. and Nogues, M. V. (2003) Both aromatic and cationic residues contribute to the membrane-lytic and bactericidal activity of eosinophil cationic protein. Biochemistry **42**, 6636–6644

29 Yang, J. T., Wu, C. S. and Martinez, H. M. (1986) Calculation of protein conformation from circular dichroism. Methods Enzymol. **130**, 208–269

30 Conchillo-Sole, O., de Groot, N. S., Aviles, F. X., Vendrell, J., Daura, X. and Ventura, S. (2007) AGGRESCAN: a server for the prediction and evaluation of 'hot spots' of aggregation in polypeptides. BMC Bioinformatics **8**, 65

31 Hilpert, K., Volkmer-Engert, R., Walter, T. and Hancock, R. E. (2005) High-throughput generation of small antibacterial peptides with improved activity. Nat. Biotechnol. **23**, 1008–1012

32 Carreras, E., Boix, E., Navarro, S., Rosenberg, H. F., Cuchillo, C. M. and Nogues, M. V. (2005) Surface-exposed amino acids of eosinophil cationic protein play a critical role in the inhibition of mammalian cell proliferation. Mol. Cell. Biochem. **272**, 1–7

33 Marshall, G. R., Feng, J. A. and Kuster, D. J. (2008) Back to the future: ribonuclease A. Biopolymers **90**, 259–277

34 Reshetnyak, Y. K., Koshevnik, Y. and Burstein, E. A. (2001) Decomposition of protein tryptophan fluorescence spectra into log-normal components. III. Correlation between fluorescence and microenvironment parameters of individual tryptophan residues. Biophys. J. **81**, 1735–1758

35 Nikolovski, Z., Buzon, V., Ribo, M., Moussaoui, M., Vilanova, M., Cuchillo, C. M., Cladera, J. and Nogues, M. V. (2006) Thermal unfolding of eosinophil cationic protein/ribonuclease 3: a nonreversible process. Protein Sci. **15**, 2816–2827

36 Boix, E., Leonidas, D. D., Nikolovski, Z., Nogues, M. V., Cuchillo, C. M. and Acharya, K. R. (1999) Crystal structure of eosinophil cationic protein at 2.4 Å resolution. Biochemistry **38**, 16794–16801

37 Venge, P., Bystrom, J., Carlson, M., Hakansson, L., Karawacjzyk, M., Peterson, C., Seveus, L. and Trulson, A. (1999) Eosinophil cationic protein (ECP): molecular and biological properties and the use of ECP as a marker of eosinophil activation in disease. Clin. Exp. Allergy **29**, 1172–1186

38 Zhang, J., Rosenberg, H. F. and Nei, M. (1998) Positive Darwinian selection after gene duplication in primate ribonuclease genes. Proc. Natl. Acad. Sci. U.S.A. **95**, 3708–3713

39 Brown, K. L. and Hancock, R. E. (2006) Cationic host defense (antimicrobial) peptides. Curr. Opin. Immunol. **18**, 24–30

40 Andreu, D. and Rivas, L. (1998) Animal antimicrobial peptides: an overview. Biopolymers **47**, 415–433

41 Bulet, P., Stocklin, R. and Menin, L. (2004) Anti-microbial peptides: from invertebrates to vertebrates. Immunol. Rev. **198**, 169–184

42 Nitto, T., Dyer, K. D., Czapiga, M. and Rosenberg, H. F. (2006) Evolution and function of leukocyte RNase A ribonucleases of the avian species, *Gallus gallus*. J. Biol. Chem. **281**, 25622–25634

43 Huang, Y. C., Lin, Y. M., Chang, T. W., Wu, S. J., Lee, Y. S., Chang, M. D., Chen, C., Wu, S. H. and Liao, Y. D. (2007) The flexible and clustered lysine residues of human ribonuclease 7 are critical for membrane permeability and antimicrobial activity. J. Biol. Chem. **282**, 4626–4633

44 Schroder, J. M. and Harder, J. (2006) Antimicrobial skin peptides and proteins. Cell. Mol. Life Sci. **63**, 469–486

45 Fan, T. C., Fang, S. L., Hwang, C. S., Hsu, C. Y., Lu, X. A., Hung, S. C., Lin, S. C. and Chang, D. T. (2008) Characterization of molecular interactions between eosinophil cationic protein and heparin. J. Biol. Chem. **283**, 25468–25474

46 Ulrich, M., Petre, A., Youhnovski, N., Promm, F., Schirle, M., Schumm, M., Pero, R. S., Doyle, A., Checkel, J., Kita, H. et al. (2008) Post-translational tyrosine nitration of eosinophil granule toxins mediated by eosinophil peroxidase. J. Biol. Chem. **283**, 28629–28640

47 Gorr, S. U., Sotsky, J. B., Shelar, A. P. and Demuth, D. R. (2008) Design of bacteria-agglutinating peptides derived from parotid secretory protein, a member of the bactericidal/permeability increasing-like protein family. Peptides **29**, 2118–2127

online data

SUPPLEMENTARY ONLINE DATA

Bactericidal and membrane disruption activities of the eosinophil cationic protein are largely retained in an N-terminal fragment

Marc TORRENT*, Beatriz G. DE LA TORRE†, Victòria M. NOGUÉS*, David ANDREU† and Ester BOIX*[1]

*Department Bioquímica i Biologia Molecular, Fac. Biociències, Universitat Autònoma de Barcelona, Cerdanyola del Vallès, Spain, and † Department Ciències Experimentals i de la Salut, Universitat Pompeu Fabra-Parc de Recerca Biomèdica de Barcelona, Barcelona, Spain

SUPPLEMENTAL EXPERIMENTAL

Chemicals used for peptide synthesis, analysis and purification

Fmoc (fluoren-9-ylmethoxycarbonyl)-protected amino acids were obtained from Senn Chemicals or Iris Biotech; MBHA (Fmoc-Rink-amide) resin and MBHA linker were from Nova-biochem; and HBTU [2-(1H-benzotriazol-1-yl)-1,1,3,3-tetra-methyluronium hexafluorophosphate] and HOBt (N-hydroxy-benzotriazole) were from Matrix Innovation. HPLC-grade acetonitrile, and peptide synthesis grade DMF (N,N-dimethyl-formamide), DCM (dichloromethane), DIEA (N,N-diisopropyl-ethylamine) and TFA (trifluoroacetic acid) were from SDS (Peypin, France).

Peptide synthesis, analysis and purification

Solid-phase synthesis of peptides ECP-(24–45) and ECP-(1–45) was done by Fmoc-based chemistry on MBHA resin (0.1 mmol) in a model 433A peptide synthesizer (Applied Biosystems) running FastMoc protocols. Couplings used an 8-fold molar excess each of Fmoc amino acid, HBTU and HOBt, and 16-fold molar excess of DIEA. Side-chain protecting groups were t-butyl (Ser, Thr and Tyr), t-butyloxycarbonyl (Lys and Trp), 2,2,4,6,7-pentamethyldihydrobenzofuran-5-sulfonyl (Arg), and trityl (Asn, Gln and His). After chain assembly, full deprotection and cleavage was carried out with TFA/water/triisopropylsilane (95:2.5:2.5, v/v, for 90 min at room temperature). Peptides were precipitated by addition of chilled methyl t-butyl ether,
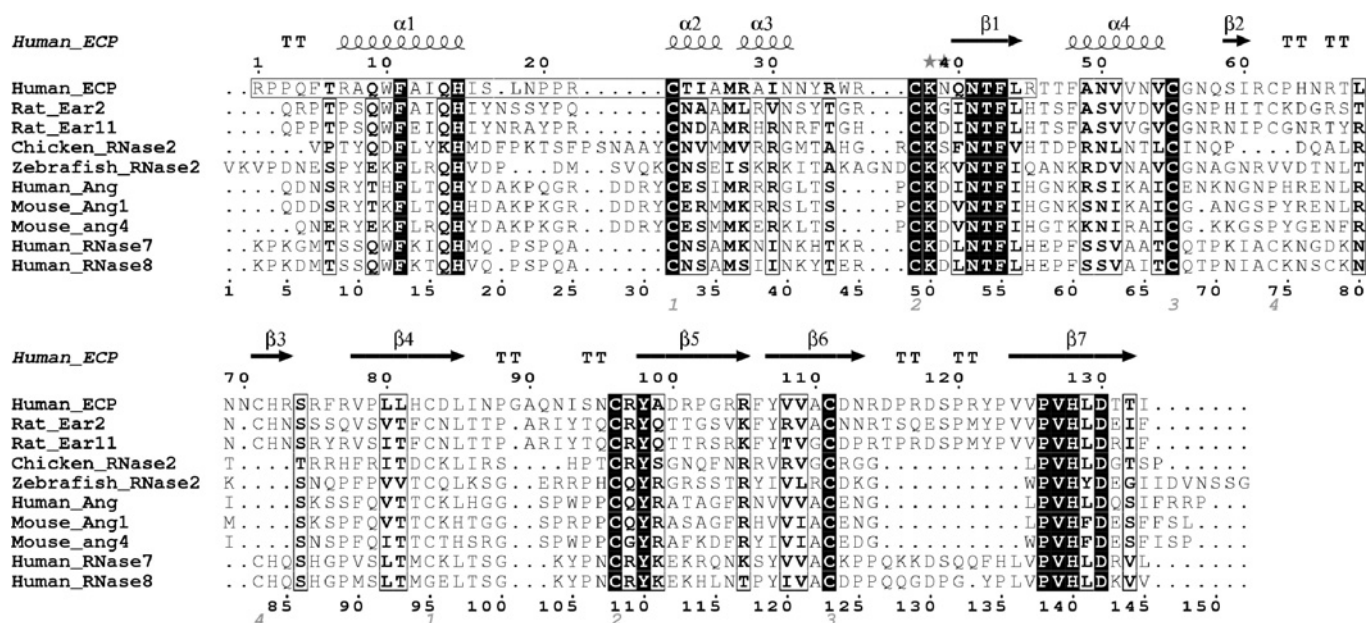

Figure S1   Alignment of ECP and other RNase A family members with described antimicrobial activity

The secondary structure of ECP is indicated. The studied N-terminal fragment (residues 1–45) is boxed. Alignments were performed with ClustalW and the picture was drawn using the ESprit software. Strictly conserved residues are framed in black and conserved residues in most of the sequences, as calculated by a similarity score, are boxed. Disulfide bond pairing is shown at the bottom. Primary sequences correspond to the mature protein, and are taken from the following Swiss-Prot accession numbers: RNase 1 (P07998); RNase 2 (P47780); RNase 3 (P12724); RNase 4 (P34096); RNase 5 (P03950); RNase 6 (P47778); RNase 7 (Q9H1E1); RNase 8 (Q8TDE3); eosinophil associated Ear2 (Q5WN11); eosinophil associated Ear11 (P70709); mouse angiogenin 1 (P21570); mouse angiogenin 4 (Q80Z85); chicken leucocyte RNase A-2 (Q27J90); and zebrafish Dr-RNase 2 (ABQ2378).

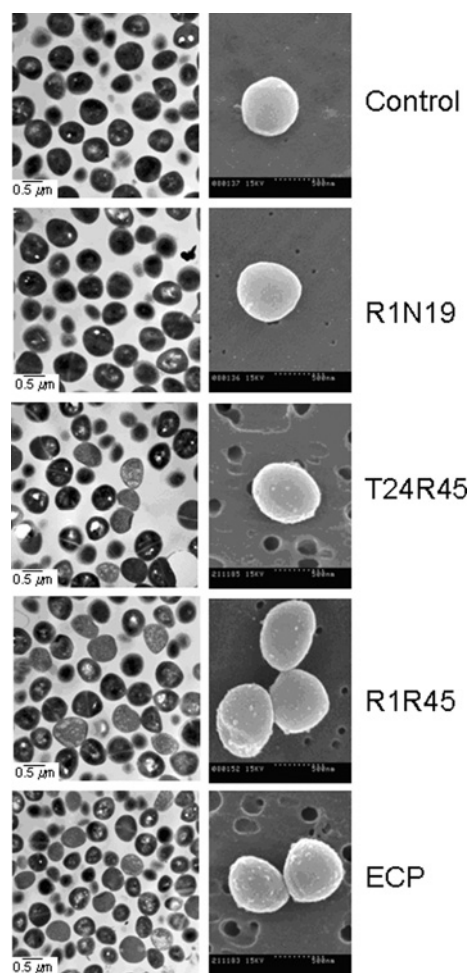[1] To whom correspondence should be addressed (email ester.boix@uab.es).

Figure S2 TEM and SEM of *S. aureus* incubated with ECP or ECP-derived peptides

Left-hand panel, TEM. Right-hand panel, SEM. Each sample was incubated with 10 μM of ECP or ECP peptides for 3 h. From top to bottom: control cells; ECP-(1–19), R1N19; ECP-(24–45), T24R45; ECP-(1–45), R1R45; and ECP.

Figure S3 Displacement of LPS-bound BC by ECP and its derived peptides

ECP, (◆); ECP-(1–45), (▲); ECP-(24–45), (●); ECP-(1–19) (■) and polymyxin B (▽). LPS at 10 μg/ml and BC at 10 μM final concentrations were diluted in 5 mM Hepes/KOH, pH 7.5. BC displacement, evidenced as unquenching of the fluorescence signal, is quantified by its occupancy factor, as detailed in the Experimental section of the main paper.

taken up in aqueous HOAc (0.1 M) and lyophilized. Analytical reversed-phase HPLC was performed on a Luna C_{18} column (4.6 mm × 50 mm, 3 μm; Phenomenex). Linear gradients of solvent B (0.036 % TFA in acetonitrile) into solvent A (0.045 % TFA in water) were used for elution, as indicated in Table S1, at a flow rate of 1 ml/min, and with UV detection at 220 nm. Preparative HPLC runs were performed on a Luna C_{18} column (21.2 mm × 250 mm, 10 μm; Phenomenex), using linear gradients of solvent B (0.1 % in acetonitrile) into solvent A (0.1 % TFA in water), as required, with a flow rate of 25 ml/min. MALDI–TOF-MS (matrix-assisted laser-desorption ionization–time-of-flight MS) spectra were recorded in the reflector mode in a Voyager DE-STR workstation (Applied Biosystems) using α-hydroxycinnamic acid matrix. Fractions of adequate (> 90 %) HPLC homogeneity and with the expected mass were pooled and lyophilized for subsequent experiments.
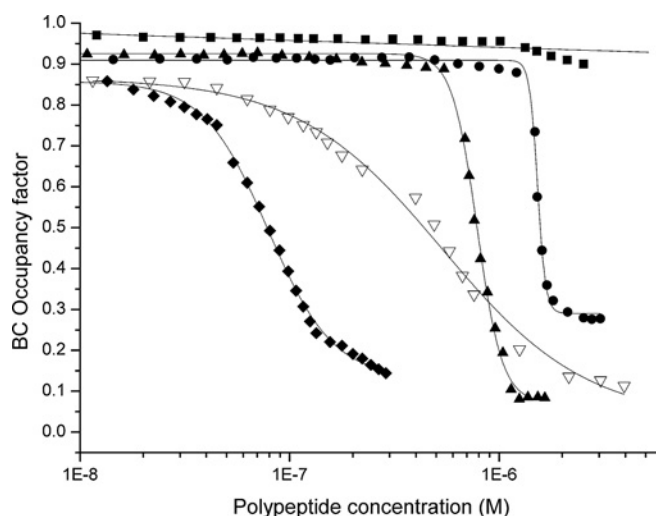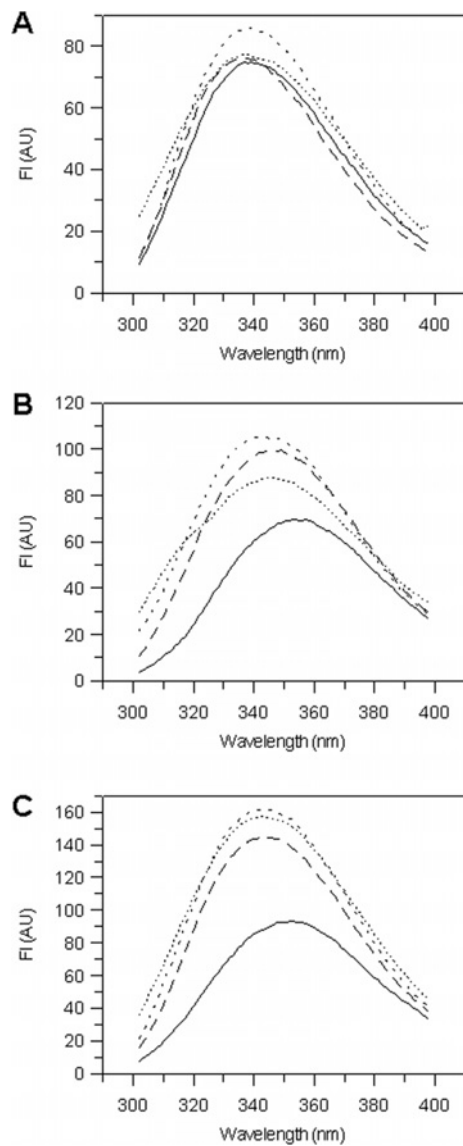
Figure S4   Comparison of the fluorescence emission spectra of ECP and its derived peptides

(**A**) ECP-(1–19). (**B**) ECP-(24–45). (**C**) ECP-(1–45). Absence (solid line) and presence of 3:2 DOPC/DOPG liposomes (- - - - -), LPS (-- - -- - -) and LTA (·····), as described in the Experimental section of the main paper. For each condition three spectra were averaged.
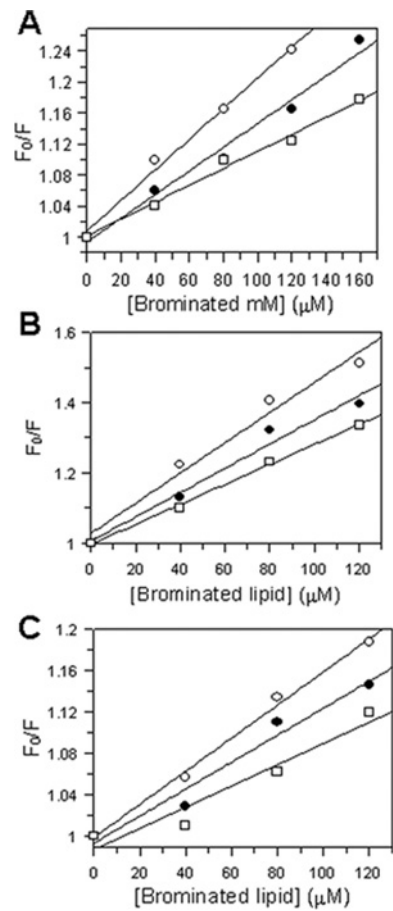

Figure S5   Stern–Volmer plots for the depth-dependent quenching of tryptophan fluorescence

(**A**) ECP-(1–19). (**B**) ECP-(24–45). (**C**) ECP-(1–45). Liposomes containing DOPC/DOPG (3:2) were mixed with increasing molar ratios of (6,7)-Br_2PC (○), (9,10)-Br_2PC (●), or (11,12)-Br_2PC (□). Assay conditions were 0.5 μM final protein concentration and 200 μM liposome concentration.
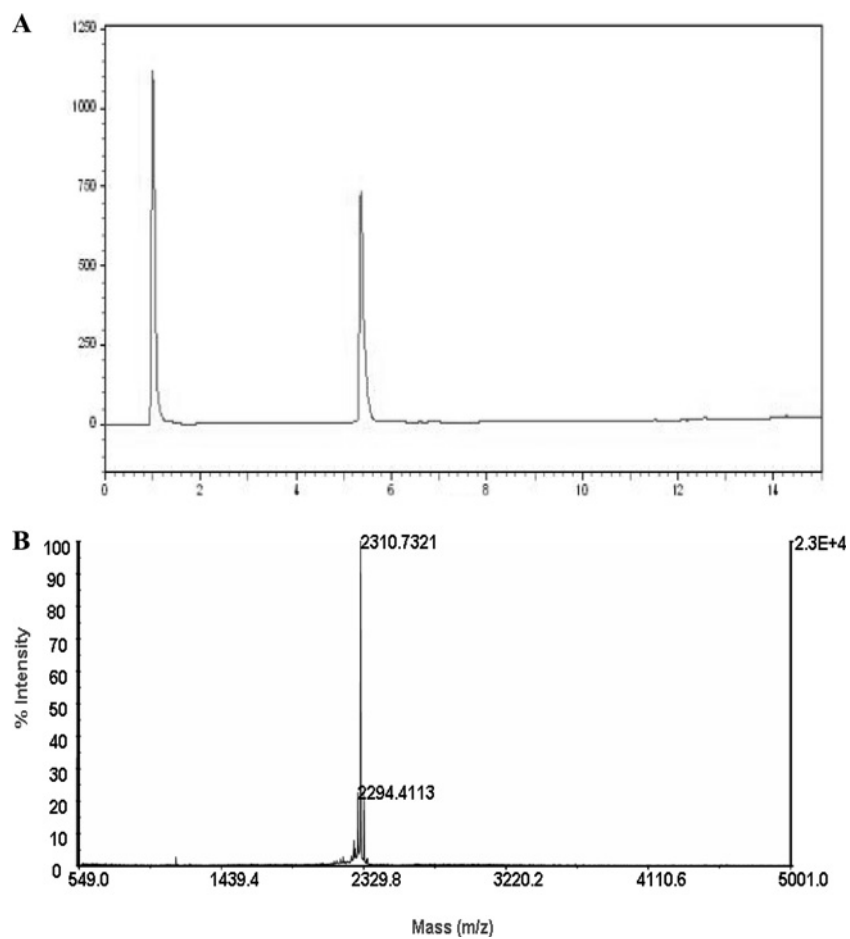
Figure S6   HPLC and mass spectra of ECP-(1–19)

(**A**) Reversed-phase HPLC, 20–45 % acetonitrile in 15 min (**B**) MALDI–TOF-MS (reflector mode). Sequence of peptide, RPPQFTRAQWFAIQHISLN; molecular mass, 2309.22 Da (monoisotopic).
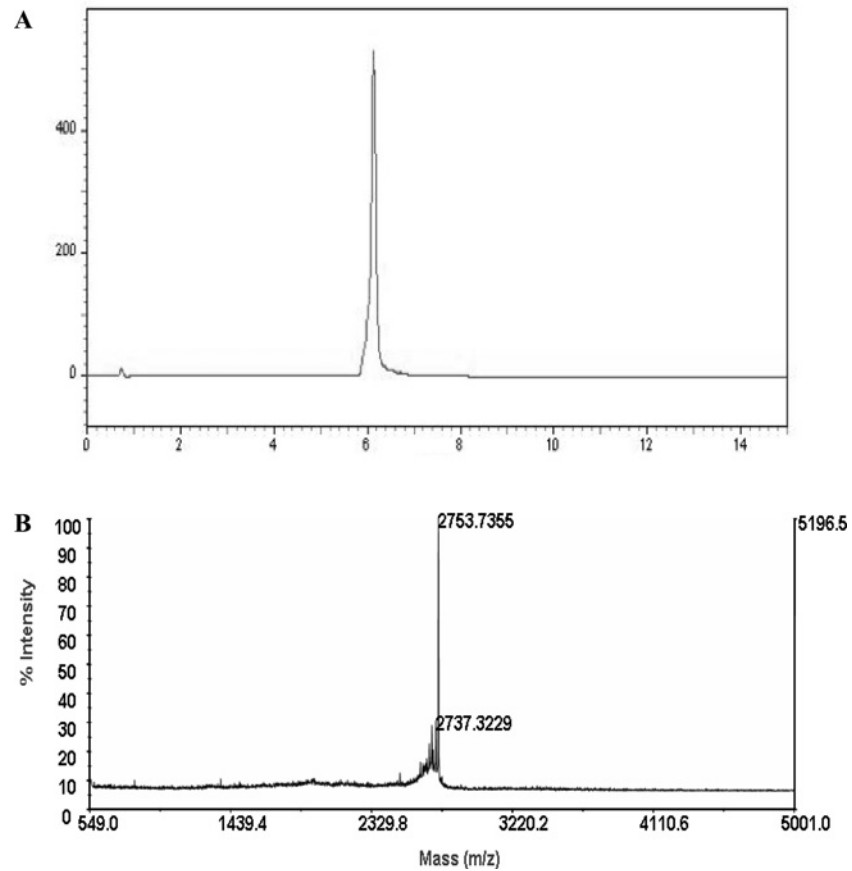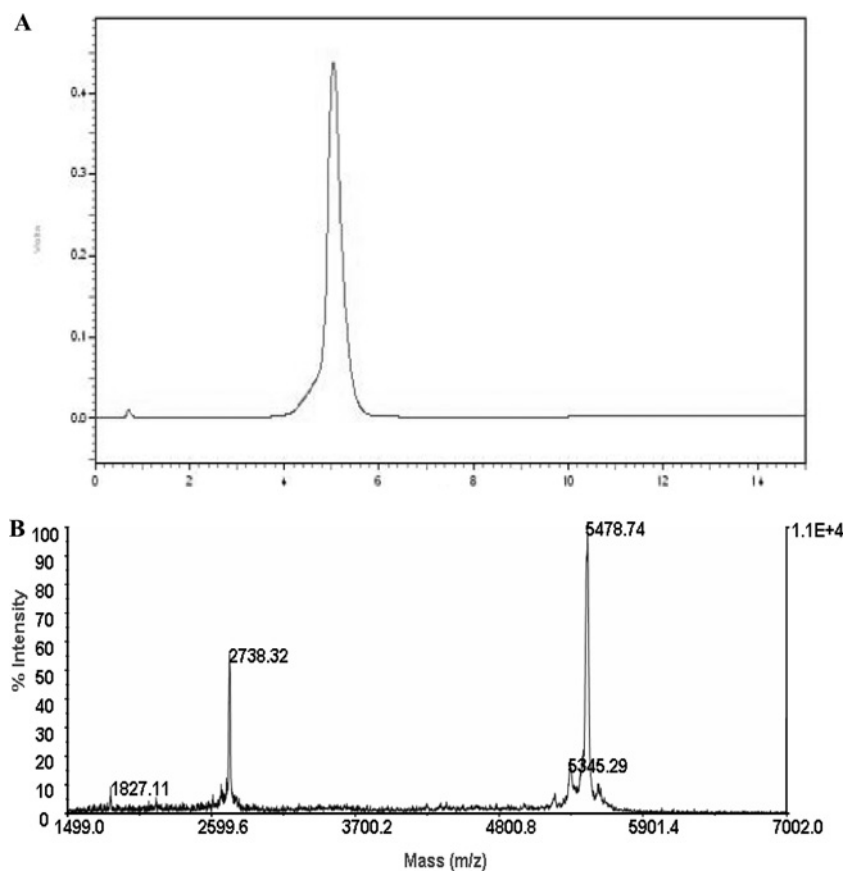
Figure S7   HPLC and mass spectra of ECP-(24–45)

(**A**) Reversed-phase HPLC, 20–45 % MeCN in 15 min. (**B**) MALDI–TOF-MS. Sequence of peptide, TIAMRAINNYRWRSKNQNTFLR-amide; molecular mass, 2752.45 Da (monoisotopic).

Figure S8   HPLC and mass spectra of ECP-(1–45)

(**A**) Reversed-phase HPLC, 20–45 % MeCN in 15 min. (**B**) MALDI-TOF MS (linear mode). Sequence of peptide, RPPQFTRAQWFAIQHISLNPPRSTIAMRAINNYRWRSKNQNTFLR-amide; molecular mass, 5483.3 Da (average).